Green Chemistry

Accepted Manuscript

ROYAL SOCIETY OF CHEMISTRY

www.rsc.org/greenchem

Green Chemistry

RSCPublishing

ARTICLE

Ammonia-Free Coprecipitation Synthesis of Ni-Co-Mn Hydroxides Precursor for High-Performance Battery Cathode Materials

Cite this: DOI: 10.1039/x0xx00000x

Received 00th January 2012,
Accepted 00th January 2012

DOI: 10.1039/x0xx00000x

www.rsc.org/

Kyoung-Mo Nam, ‖[a] Hyun-Jin Kim, ‖[a] Dong-Hyun Kang,[b] Yong-Seok Kim[b] and Seung-Wan Song[a]*

Ammonia-free green coprecipitation process has successfully produced micro-sized spherical $Ni_{0.5}Co_{0.2}Mn_{0.3}(OH)_2$ precursor with a homogeneous elemental distribution. The replacement of ammonia with citric acid as a chelating agent was the key for this eco-friendly and cost-effective process. The pH of coprecipitation was determined from solubility and complex formation diagrams calculated by using solubility products and formation constants. With varying the relative ratio of citric acid to metals, optimized particle morphology, size and robustness of the precursor were obtained. The cathode material $LiNi_{0.5}Co_{0.2}Mn_{0.3}O_2$, prepared using hydroxides coprecipitate precursor, showed a good charge-discharge cycling performance in lithium cells, delivering high capacity and cycling stability (≥ 94% retention) at 3.0 - 4.3 V as well as upon high-voltage operation to 4.6 V.

Introduction

Rapidly growing needs of high-energy density Li-ion batteries for electric vehicle and grid-based energy storage systems require the development of higher-voltage and higher-capacity cathode materials than current ones. The Ni-rich layered oxide cathode materials of $Li(Ni_{1-x-y}Co_xMn_y)O_2$ ($0 \le x \le 1$, $0 \le y \le 1$, NCM) are promising candidates for high-energy density battery applications, because of their large capacity of ≈ $200mAhg^{-1}$.[1,2] Commercial NCMs (e.g., $LiNi_{1/3}Co_{1/3}Mn_{1/3}O_2$, $LiNi_{0.5}Co_{0.2}Mn_{0.3}O_2$) are known to be often manufactured by calcining the powders of lithium salt and metal hydroxides ($(Ni_{1-x-y}Co_xMn_y)(OH)_2$) coprecipitate precursor that possesses a homogeneous distribution of three metals and spherical secondary micro-sized particles consisting of smaller primary particles. These material specifications provide a phase-pure final product and a satisfied packing density of the cathode material in contrast to those in irregular particle shape and size or nanoparticles, respectively.[1,3-7]

In the preparation of $(Ni_{1-x-y}Co_xMn_y)(OH)_2$ coprecipitate precursor, the major difficulty is that Mn^{2+}can easily be oxidized to Mn^{3+}or Mn^{4+} in the air, causing the formation of other phases, and uncontrolled stoichiometry and particle morphology. Hence, the use of a chelating agent, together with a closed reactor that can block the air, is necessary to obtain a homogeneous mixing of metal cations in aqueous solution through the formation of metal-ligand complex and to prevent the phase separation. Then, homogeneous and stoichiometric metal hydroxides coprecipitate is obtainable.

Widely used coprecipiation synthesis of metal hydroxides includes the use of ammonia as a chelating agent[4,5,7-14] forming transition metal-ammonia complexes and proceeds in two steps; first, metal ions form the complex with ammonia aqueous solution, in which more than 0.2 M of ammonia water is used, as represented in the equation (1). Then, by anion-exchange from ammonia to hydroxide anions that come from NaOH added, metal hydroxides precipitate slowly as in the equation (2).[7,8,15]

$$M^{2+} + nNH_4OH \rightarrow [M(NH_3)_n]^{2+} + 2H_2O \quad (1)$$

$$[M(NH_3)_n]^{2+} + 2OH^- + nH_2O \rightarrow M(OH)_2 + nNH_4OH \quad (2)$$

Such stepwise processes promote first the formation of small primary particles, followed by the formation of secondary particles by aggregation (Ostwald ripening) of existing primary particles. Then, micro-sized secondary particles consisting of smaller or nano-sized primary particles are produced. If the metal ions reacted directly with NaOH solution in the absence of ammonia, the reaction is too fast to control the reaction kinetics, which may not produce secondary particles but just small primary particles with poor density and inhomogeneous chemical composition.

Ammonia in aqueous solution evaporates easily to gaseous phase, readily oxidizes to either nitrite (NO_2^-) or nitrate (NO_3^-) under

[a]Department of Fine Chemical Engineering & Applied Chemistry, Chungnam National University, Daejeon 305-764, Republic of Korea.
E-mail:swsong@cnu.ac.kr; Fax: (+82) 42-821-6637
[b]EMT Co., Ltd, Chumgju 380-871, Republic of Korea

‖ These authors contributed equally.

aerobic conditions[16,17] and produces its derivatives of nitrogen (-NH_2-, NH_3, NH_4^+)-containing chemical waste products.[18,19] These characteristics cause the pollutions of water, soil and air, and the pollution events directly threaten the life systems. Thus, ammonia is defined as a toxic material by inhalation and requires a hazardous safety permit. The level of ammonia is being regulated universally. In those environmental view points, it is better not to use ammonia and/or reduce the amount of ammonia in any chemical processing. Also importantly, no use of ammonia is economical; no extra charge for the treatment of nitrogen-containing chemical waste products is needed.[20] In order to reduce ammonia-induced pollutions and cost in the coprecipitation synthetic process, the simplest way is to develop ammonia-free process.

Here, we report ammonia-free low-cost coprecipitation synthesis of multicomponent metal hydroxides precursor, utilizing a small amount of citric acid as a new chelating agent. The optimum pH was determined based on the theoretical calculation of solubility and complex formation of individual metal hydroxides and citrates, respectively. The electrochemical characteristics of the resulting cathode material, which is synthesized using metal hydroxides precursor coprecipitated using citric acid, are discussed. We suggest our ammonia-free coprecipitation method as a novel route for producing high-performance battery cathodes.

Theoretical calculation of solubilities

Coprecipitation synthesis using citric acid starts from the formation of metal-citrate complex (equation (3)),[21] where metal cations are coordinated by the ligands of citrate anion. Then, the citrate anions are slowly replaced by hydroxide anions coming from NaOH, *via* anion-exchange reaction, forming metal-hydroxides coprecipitate (equation (4)),[22] as illustrated in Scheme 1.

$$M^{2+} + C_6H_5O_7^{3-} \leftrightarrows [M(C_6H_5O_7)]^- \quad (3)$$

$$[M(C_6H_5O_7)]^- + 2OH^- \leftrightarrows M(OH)_2 + C_6H_5O_7^{3-} \quad (4)$$

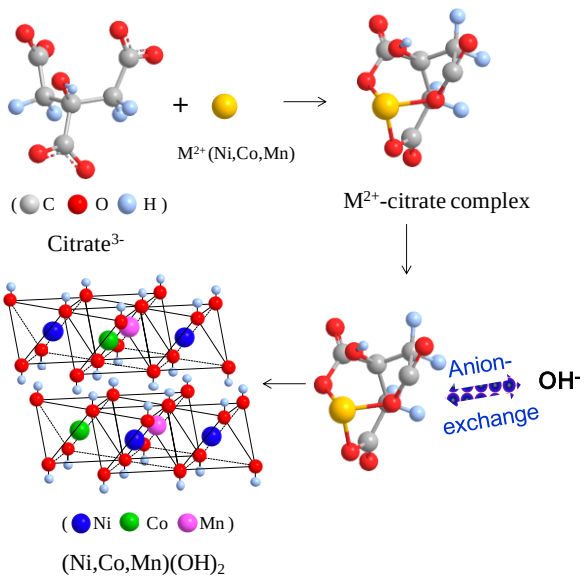

Scheme 1. Coprecipitation synthesis of metal hydroxides using citric acid as a chelating agent *via* anion-exchange reaction.

Table 1. Reactions and equilibrium constants used in the solubility calculations.[a]

	Reactions	Equilibrium constants[b]	log K	ref
1	$C_6H_8O_7 \leftrightarrows C_6H_7O_7^- + H^+$	K_1	-3.1	24
2	$C_6H_7O_7^- \leftrightarrows C_6H_6O_7^{2-} + H^+$	K_2	-4.8	24
3	$C_6H_6O_7^{2-} \leftrightarrows C_6H_5O_7^{3-} + H^+$	K_3	-6.4	24
4	$Ni^{2+} + 2H^+ + C_6H_5O_7^{3-} \leftrightarrows Ni\text{-}H_2C_6H_5O_7^+$	K_{f1}	12.9	24
5	$Ni^{2+} + H^+ + C_6H_5O_7^{3-} \leftrightarrows Ni\text{-}HC_6H_5O_7$	K_{f2}	10.5	24
6	$Ni^{2+} + C_6H_5O_7^{3-} \leftrightarrows Ni\text{-}C_6H_5O_7^-$	K_{f3}	6.7	24
7	$Co^{2+} + 2H^+ + C_6H_5O_7^{3-} \leftrightarrows Co\text{-}H_2C_6H_5O_7^+$	K_{f1}	12.9	24
8	$Co^{2+} + H^+ + C_6H_5O_7^{3-} \leftrightarrows Co\text{-}HC_6H_5O_7$	K_{f2}	10.3	24
9	$Co^{2+} + C_6H_5O_7^{3-} \leftrightarrows Co\text{-}C_6H_7O_7^-$	K_{f3}	6.3	24
10	$Mn^{2+} + H^+ + C_6H_5O_7^{3-} \leftrightarrows Mn\text{-}HC_6H_5O_7$	K_{f1}	9.4	24
11	$Mn^{2+} + C_6H_5O_7^{3-} \leftrightarrows Mn\text{-}C_6H_7O_7^-$	K_{f2}	5.5	24
12	$Ni^+ + H_2O \leftrightarrows NiOH^+ + H^+$	K_1	-9.9	25
13	$Ni^+ + 2H_2O \leftrightarrows Ni(OH)_2 + 2H^+$	K_2	-19.0	25
14	$Ni^+ + 3H_2O \leftrightarrows Ni(OH)_3^- + 3H^+$	K_3	-30.0	25
15	$Ni^+ + 4H_2O \leftrightarrows Ni(OH)_4^{2-} + 4H^+$	K_4	-44.0	25
16	$2Ni^{2+} + H_2O \leftrightarrows Ni_2OH^{3+} + H^+$	K_5	-10.7	25
17	$4Ni^{2+} + 4H_2O \leftrightarrows Ni_4(OH)_4^{4+} + 4H$	K_6	-27.7	25
18	$Ni(OH)_2(s) + 2H^+ \leftrightarrows Ni^{2+} + 2H_2O$	K_{sp}	-17.2	25
19	$Co^+ + H_2O \leftrightarrows CoOH^+ + H^+$	K_1	-9.7	25
20	$Co^+ + 2H_2O \leftrightarrows Co(OH)_2 + 2H^+$	K_2	-18.8	25
21	$Co^+ + 3H_2O \leftrightarrows Co(OH)_3^- + 3H^+$	K_3	-31.5	25
22	$Co^+ + 4H_2O \leftrightarrows Co(OH)_4^{2-} + 4H^+$	K_4	-46.3	25
23	$2Co^{2+} + H_2O \leftrightarrows Co_2OH^{3+} + H^+$	K_5	-11.2	25
24	$4Co^{2+} + 4H_2O \leftrightarrows Co_4(OH)_4^{4+} + 4H$	K_6	-30.5	25
25	$Co(OH)_2(s) + 2H^+ \leftrightarrows Co^{2+} + 2H_2O$	K_{sp}	-15.7	25
26	$Mn^{2+} + H_2O \leftrightarrows MnOH^+ + H^+$	K_1	-15.2	25
27	$2Mn^{2+} + H_2O \leftrightarrows MnOH^{3+} + H^+$	K_2	-10.6	25
28	$2Mn^{2+} + 3H_2O \leftrightarrows Mn_2(OH)_3^+ + 3H^+$	K_3	-10.6	25
29	$Mn^{2+} + 4H_2O \leftrightarrows Mn_2(OH)_4^{2-} + 4H^+$	K_4	-23.9	25
30	$Mn^{2+} + 2H_2O \leftrightarrows Mn(OH)_2 + 2H^+$	K_5	-48.3	25
31	$Mn^{2+} + 3H_2O \leftrightarrows Mn(OH)_3^- + 3H^+$	K_6	-22.2	25
32	$Mn(OH)_2(s) + 2H^+ \leftrightarrows Mn^{2+} + 2H_2O$	K_{sp}	-15.2	25

[a] Reaction conditions: T= 25°C, P= 1atm. [b] The values are given as logarithms of the overall equilibrium constants.

As the pH for the formation of metal-citrate complex and -hydroxide precipitate can be different for each metals, it is important to calculate the solubility behavior of each metal and determine the optimum pH for the coprecipitation of Ni-Co-Mn hydroxides in the presence of metal-citrate complexes.[23] The pH is theoretically calculated based on the chemical species present in water with respect to pH, the concentration of metal ions and their thermodynamic equilibrium constants.[22] Chemical equilibrium used for the calculation are listed in Table 1. The solubility diagrams are plotted with the logarithmic molar concentration calculated as a function of pH.

Formation of metal-citrate complexes

The variation of the concentration of citrate species is obtained by solving the equilibrium equations that are pH-dependent dissociation of citric acid in water (reactions 1-3 in Table 1).

$$C_6H_8O_7 \leftrightarrows C_6H_7O_7^- + H^+ \quad K_1 = 10^{-3.1}$$

$$K_1 = \frac{[C_6H_7O_7^-][H^+]}{[C_6H_8O_7]} \rightarrow [C_6H_7O_7^-] = \frac{K_1[C_6H_8O_7]}{[H^+]} \quad (5)$$

$$C_6H_7O_7^- \leftrightarrows C_6H_6O_7^{2-} + H^+ \quad K_2 = 10^{-4.8}$$

$$K_2 = \frac{[C_6H_6O_7^{2-}][H^+]}{[C_6H_7O_7^-]} \rightarrow [C_6H_6O_7^{2-}] = \frac{K_2[C_6H_7O_7^-]}{[H^+]}$$

$$\rightarrow [C_6H_6O_7^{2-}] = \frac{K_1K_2[C_6H_8O_7]}{[H^+]^2} \quad (6)$$

$$C_6H_6O_7^{2-} \leftrightarrows C_6H_5O_7^{3-} + H^+ \quad K_3 = 10^{-6.4}$$

$$K_3 = \frac{[C_6H_5O_7^{3-}][H^+]}{[C_6H_6O_7^{2-}]} \rightarrow [C_6H_5O_7^{3-}] = \frac{K_3[C_6H_6O_7^{2-}]}{[H^+]}$$

$$\rightarrow [C_6H_5O_7^{3-}] = \frac{K_1K_2K_3[C_6H_8O_7]}{[H^+]^3} \quad (7)$$

Using reactions 4-6 in Table 1, the complex formation between Ni cation and citrate anion in aqueous solution is calculated as the following.

$$Ni^{2+} + 2H^+ + C_6H_5O_7^{3-} \leftrightarrows Ni\text{-}H_2C_6H_5O_7^+ \quad K_{f1} = 10^{12.9}$$

$$K_{f1} = \frac{[NiH_2C_6H_5O_7^+]}{[Ni^{2+}][H^+]^2[C_6H_5O_7^{3-}]}$$

$$\rightarrow [NiH_2C_6H_5O_7^+] = K_{f1}[Ni^{2+}][H^+]^2[C_6H_5O_7^{3-}] \quad (8)$$

$$Ni^{2+} + H^+ + C_6H_5O_7^{3-} \leftrightarrows Ni\text{-}HC_6H_5O_7 \quad K_{f2} = 10^{10.5}$$

$$K_{f2} = \frac{[NiHC_6H_5O_7]}{[Ni^{2+}][H^+][C_6H_5O_7^{3-}]}$$

$$\rightarrow [NiHC_6H_5O_7] = K_{f2}[Ni^{2+}][H^+][C_6H_5O_7^{3-}] \quad (9)$$

$$Ni^{2+} + C_6H_5O_7^{3-} \leftrightarrows Ni\text{-}C_6H_5O_7^- \quad K_{f3} = 10^{6.7}$$

$$K_{f3} = \frac{[NiC_6H_5O_7^-]}{[Ni^{2+}][C_6H_5O_7^{3-}]}$$

$$\rightarrow [NiC_6H_5O_7^-] = K_{f3}[Ni^{2+}][C_6H_5O_7^{3-}] \quad (10)$$

Applying reactions (5)-(7) to reactions (8)-(10), the pH-dependent chemical equations for each metal are expressed as follows. For Ni, α_0 - α_3 correspond to the molar fractions of Ni^{2+}, $Ni\text{-}H_2C_6H_5O_7^+$, $Ni\text{-}HC_6H_5O$and $Ni\text{-}C_6H_5O_7^-$ species, respectively

$$\alpha_0 = \frac{[C_6H_8O_7]}{[C_6H_8O_7]+[C_6H_7O_7^-]+[C_6H_6O_7^{2-}]+[C_6H_5O_7^{3-}]} \quad (11)$$

$$\alpha_1 = \frac{[C_6H_7O_7^-]}{[C_6H_8O_7]+[C_6H_7O_7^-]+[C_6H_6O_7^{2-}]+[C_6H_5O_7^{3-}]} \quad (12)$$

$$\alpha_2 = \frac{[C_6H_6O_7^{2-}]}{[C_6H_8O_7]+[C_6H_7O_7^-]+[C_6H_6O_7^{2-}]+[C_6H_5O_7^{3-}]} \quad (13)$$

$$\alpha_3 = \frac{[C_6H_5O_7^{3-}]}{[C_6H_8O_7]+[C_6H_7O_7^-]+[C_6H_6O_7^{2-}]+[C_6H_5O_7^{3-}]} \quad (14)$$

The fraction diagram of Ni-citrate complex formation displayed in Figure 1a is obtained from those results. In the same way, complex formation of Co- and Mn-citrate is calculated using reactions 7-11 in Table 1 and their fraction diagrams are co-plotted in Figure 1b. The diagram indicates that the Ni-, Co- and Mn-$C_6H_5O_7^-$ complexes form mainly at pH 6 - 7.

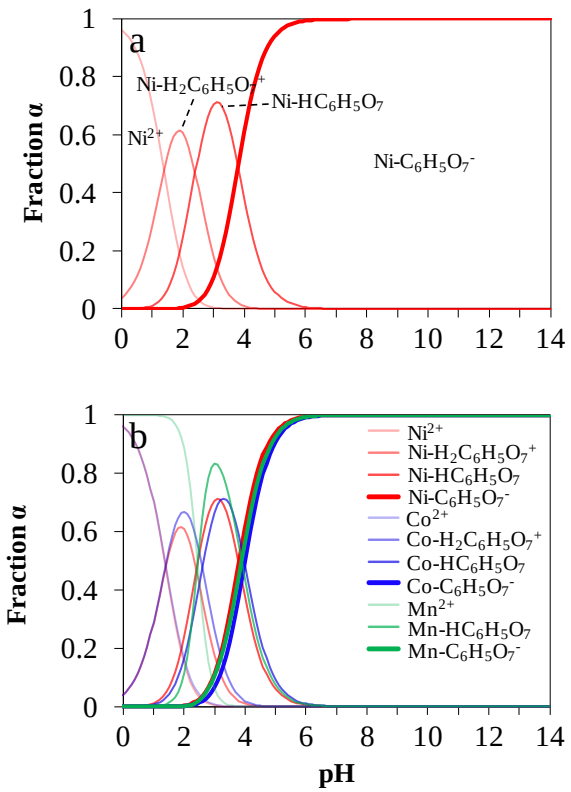

Figure 1. Fractional composition of (a) nickel- and (b) metal-citrate complex formation.

Solubility of metal hydroxides

Figure 2a shows the solubility diagram of nickel hydroxide ($Ni(OH)_2$). It is calculated from the hydrolysis reactions of possible nickel species (reactions 12-18 in Table 1).[24-27] The precipitation of $Ni(OH)_2$ begins at pH 4 and reaches to a maximum at pH 8.5 - 10 when $[Ni^{2+}]$ is 0.1 $molL^{-1}$. In the same fashion, the solubility diagrams of $Co(OH)_2$ and $Mn(OH)_2$ are obtained and co-plotted together with that of $Ni(OH)_2$ in Figure 2b. The precipitation of $Co(OH)_2$ reaches to a maximum at pH 8.5 - 12, whereas $Mn(OH)_2$ at pH 11 - 12.

The most overlapped region, which maximizes the coprecipitation, find that the optimum pH for the coprecipitation of $Ni(OH)_2$, $Co(OH)_2$ and $Mn(OH)_2$ all together is pH 10.5 –11.5, as highlighted in Figure 2b. By anion-exchange from citrate to hydroxide, the occurrence of multicomponent metal-hydroxides coprecipitation theoretically appears to be possibly made, without using ammonia.

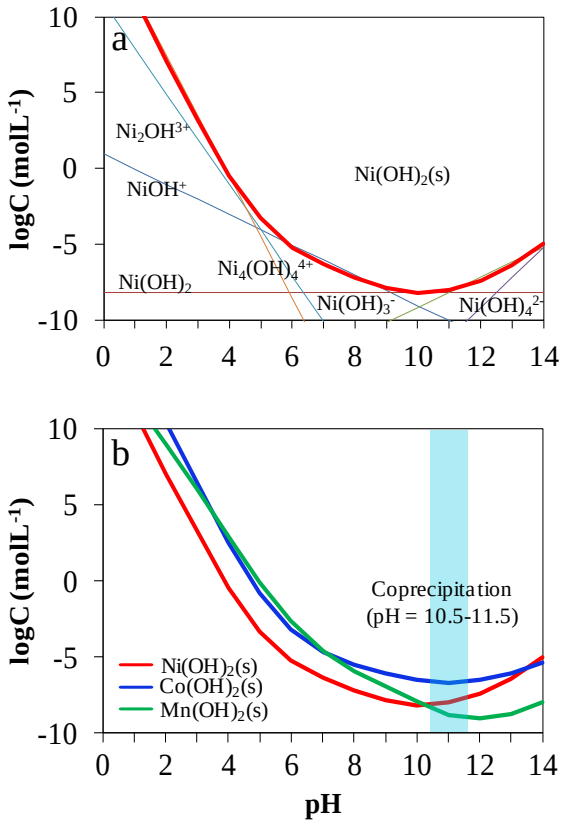

Figure 2. Solubility diagrams of (a) nickel- and (b) metal-hydroxides.

Experimental

Ammonia-free coprecipitation synthesis of metal-hydroxides precursor of $Ni_{0.5}Co_{0.2}Mn_{0.3}(OH)_2$ was conducted using citric acid at the determined optimum pH. The $NiSO_4{\cdot}6H_2O$ (99 %, Aldrich), $CoSO_4{\cdot}7H_2O$ (99 %, Aldrich) and $MnSO_4{\cdot}5H_2O$ (99 %, Aldrich) were used as the metal sources. An aqueous solution of total concentration of 1.0 M of metal sulfates, in which three metals are in the molar ratio of Ni:Co:Mn = 5:2:3, were dissolved and mixed in the distilled water. Citric acid monohydrate ($C_6H_8O_7{\cdot}H_2O$, 99.5 %, Samchun) with variable concentration of 0.01 M (P1), 0.05 M (P2), 0.5 M (P3) and 1.0 M (P4), which correspond to the same ratio of citric acid to metal, was dissolved into the aqueous solution of metal sulfates. Then, the mixed solution of metal sulfates and citric acid was slowly put into the continuous stirred tank reactor (CSTR, capacity 50L) in nitrogen atmosphere. An aqueous solution of 1.0 M NaOH (98 %, Samchun) was simultaneously fed into the reactor while controlling the pH to 11.0 at 50 °C using a pH meter. The mixture in the reactor was vigorously stirred with the stirring speed of 350 rpm as fixed. During the reaction, coprecipitation of $Ni_{0.5}Co_{0.2}Mn_{0.3}(OH)_2$ occurred. The coprecipitated solution was stirred for ~20h. Then, the coprecipitates were separated from the residual solution by a centrifuge and washed with distilled water several times until the pH of the washed solution reached 6 – 7, followed by drying in the vacuum oven at 120 °C overnight. Dark brown coprecipiate precursor powders were finally obtained.

Active cathode material of $LiNi_{0.5}Co_{0.2}Mn_{0.3}O_2$ was synthesized using the mixture of 1 mole of our coprecipitated precursor of $Ni_{0.5}Co_{0.2}Mn_{0.3}(OH)_2$ and 1.05 mole of $LiOH{\cdot}H_2O$ (99.95%, Aldrich) powders by pre-heating at 550 ℃ for 6 h and calcining at the optimized condition of 850 – 900 ℃ for 5 h in the air. The optimum synthetic condition was determined by applying variable calcination temperature (800 – 950 °C and time (5 – 10h) and by referring to previous reports.[28,29] The crystal structure of metal hydroxides coprecipitate precursors and active materials was identified with powder X-ray diffraction (XRD) analysis. XRD measurement was conducted in the 2θ range from 10° to 80° at the scan rate of 2 °/min with 0.02° step using powder X-ray diffractometer (Rigaku D/MAX-2200) with Ni-filtered Cu Kα radiation at 40 kV and 40 mA. Particle morphology and composition of the precursor and active material were examined using field-emission scanning electron microscopy (FE SEM, Hitachi) at 10 kV, SEM-energy dispersive x-ray spectroscopy (EDX, Jeol) at 10 kV and inductively coupled plasma - atomic emission spectrometer (ICP-AES, Perkin Elmer Optima-7000DV), respectively. Particle size distribution was analyzed using laser diffraction scattering method with particle size analyzer (Microtrac).

Cathodes were prepared by casting the slurry, consisting of 86 wt% $LiNi_{0.5}Co_{0.2}Mn_{0.3}O_2$ active material, 7 wt% carbon black (super P) and 7 wt% polyvinylidene fluoride (PVdF) binder in N-methyl-2-pyrrolidone (NMP, Aldrich) solvent, onto an aluminum foil to the loading level of 4 $mgcm^{-2}$, followed by vacuum drying at 60 ℃ for 2h and at 110 ℃ overnight. Electrochemical charge-discharge cycling ability of the cathode was evaluated using 2016 coin half-cells, consisting of $LiNi_{0.5}Co_{0.2}Mn_{0.3}O_2$ as a working electrode, lithium foil as a counter electrode, separator (Celgard C210) and the liquid electrolyte of 1 M $LiPF_6$/ethylene carbonate (EC) : ethylmethyl carbonate (EMC) (3:7 volume ratio, PanaX E-tec). Galvanostatic charge-discharge cycling was conducted first between 3.0 and 4.3 V at the current density of 18 mAg^{-1} (corresponding to ~0.1C) and 90 mAg^{-1} (~0.5C) using a multichannel cycler (Won-A Tech). High-voltage cycling capability of the cathode was tested between 3.0 and4.6V at 18 mAg^{-1} (~0.1C) and 36 mAg^{-1} (~0.2C), using the electrolyte containing 5 wt% methyl(2,2,2-trifluoroethyl) carbonate ($CH_3OCO_2CH_2CF_3$, FEMC, Leechem) as a high-voltage additive.[30]

Results and discussion

The coprecipitation synthesis was conducted using the variable molar ratio of citric acid to mixed metals. After the separation of the resultant precipitates, the color of residual reaction solution was however different. While for the molar ratio of 0.01 (P1) and 0.05 (P2) the residual reaction solution was transparent, for the molar ratio of 0.5 (P3) and 1.0 (P4) the color of the reaction solution was blue. The observation of such colored residual solution with the relatively higher molar ratio of 0.5 (P3) and 1.0 (P4) indicates that some metals were not coprecipitated fully but remains as cations

Table 2. Atomic ratio of coprecipitate precursors.[a]

Precursor	Molar ratio citric acid: metal	Atomic ratio[mol%] Ni	Co	Mn
P1	0.01 : 1	50.4	19.8	29.8
P2	0.05 : 1	49.8	18.4	31.8

[a] Analysis conditions: accelerating voltage= 10 kV, working distance= 10mm, vacuum level= 10^{-5}Pa.

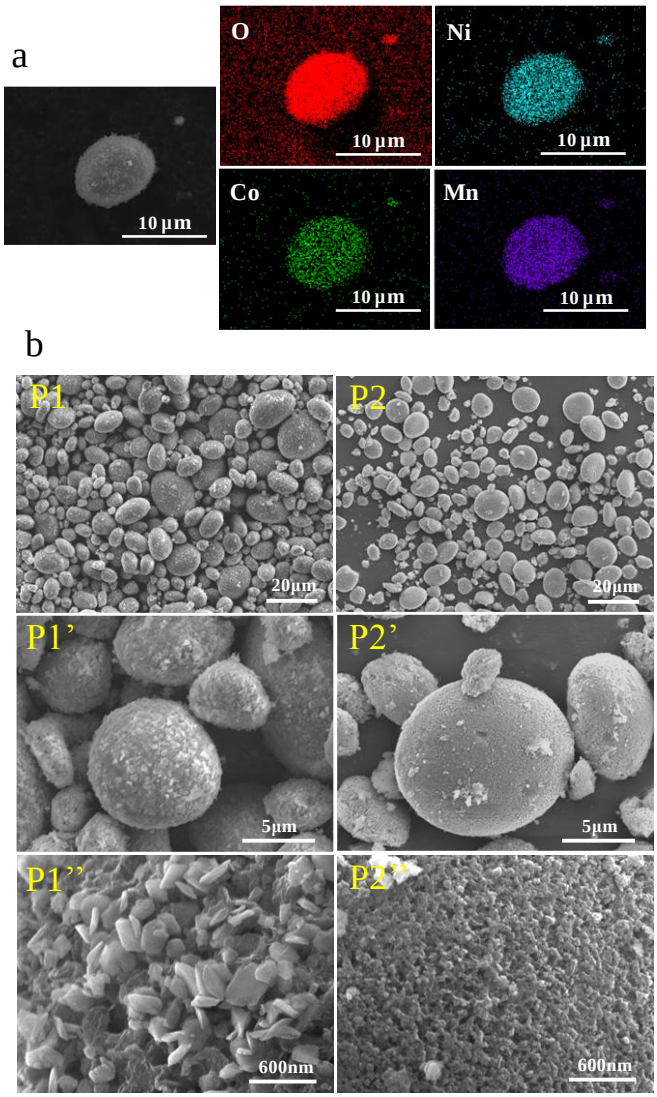

Figure 3. Elemental mapping images (a) of O, Ni, Co and Mn atoms of P1, and SEM images (b) of P1 and P2 metal-hydroxides coprecipitate precursor at different magnification.

probably as metal-citrate complexes in the reaction solution. By contrast, the use of relatively low content of citric acid, 0.01 (P1) and 0.05 (P2), is effective in coprecipitating all the metals to hydroxides.

Atomic ratios of Ni, Co and Mn of coprecipiate precursors were determined by SEM-EDX elemental mapping and the values of P1 and P2 are listed in Table 2. Measurements on several spots provide the average atomic distribution. The detection limit of SEM elemental mapping in our measurement condition is in the range of 0.2 – 0.8 wt%. The data indicate that the P1 is the stoichiometric material, whose composition is the same to the target, $Ni_{0.5}Co_{0.2}Mn_{0.3}(OH)_2$. For the P2, a little loss of cobalt compared to nickel and manganese is observed. For the P3 and P4, the loss of a lot of manganese and cobalt occurs (not shown) as predicted, being largely deviated from the target composition. Relative atomic ratio for P1 was confirmed as $Ni_{0.5}Co_{0.2}Mn_{0.3}$ using ICP-AES. Elemental mapping image of P1 (Figure 3a) reveals a uniform distribution of O (red), Ni (blue), Co (green) and Mn (purple) atoms over bulk (see scale bar of 10 m) metal hydroxides on a spherical secondary particle.

Figure 3b displays the SEM images of precursor P1 compared to the unsatisfied precursor P2. Both show spherical secondary particles in the diameter of 5 – 15 µm (P1-P1', P2-P2'), which consist of primary particles in the diameter of 300 - 500 nm on P1" and ~100 nm on P2" at a high density packing, confirmed with TEM images (not shown). The spherical secondary particle shape is known to be advantageous for fabricating highly packed (i.e., high-density) cathode.[9,31] The P1 reveals relatively more homogeneous particle size and shape, in contrast to the irregular particle shape and the presence of shapeless particles on P2.

Powder XRD patterns of precursors P1 and P2 are shown in Figure 4. For the P1, the appearance of a sharp reflection of (001) indicates its successful crystallization in an ordered layered hexagonal structure (space group *P-3ml*) of metal hydroxide.[7,8,11] For the P2, overall just broad features of reflections are observed. The broad and asymmetric peak shape is characteristic of disordered (turbostratic) structure of layered hydroxide.[32] In the ammonia-free coprecipitation, the use of a low content (0.01 M, P1) of citric acid is effective in producing crystalline metal hydroxides with appropriate particle shape and size. The use of relatively higher content (0.05 M, P2) of citric acid that has a strong complexing power to metal cations might slow down the anion exchange reaction from citrate to hydroxide anion. Then, the randomness in particle morphology and size, and poor crystallinity arise, resulting in the formation of less dense and less crystallized precursor particles.

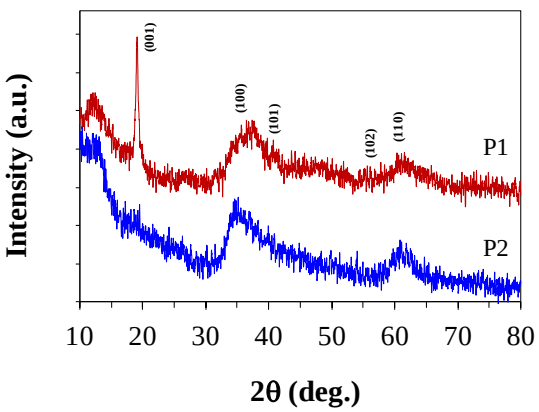

Figure 4. Powder XRD patterns of P1 and P2 metal-hydroxides coprecipitate precursorsynthesized with a differentmolar ratio of citrate to metal.

Using the precursors of P1 and P2 for comparison, cathode active materials of C1 and C2, respectively, were synthesized. Figure 5a shows their powder XRD patterns. The crystal structure of C1

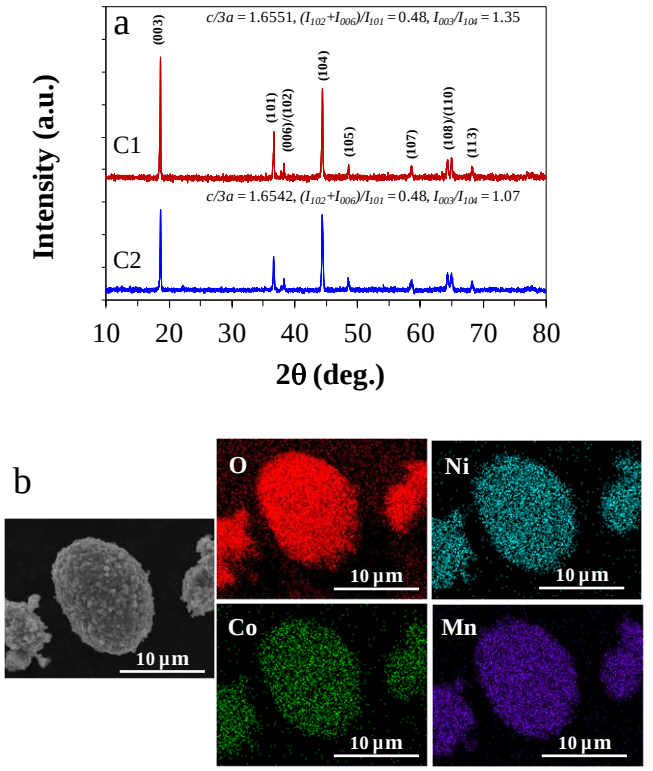

Figure 5. Powder XRD patterns of $LiNi_{0.5}Co_{0.2}Mn_{0.3}O_2$ cathode active materials (a) of C1 and C2, synthesized using P1 and P2 coprecipitate precursors, respectively, and elemental mapping images (b) of O, Ni, Co and Mn atoms of C1.

active materials was identified as hexagonal (*R3-m*), in the absence of impurity. The lattice parameters of C1 are*a* = 2.8684Å and *c* = 14.2432Å, and their ratio of *c/3a* is 1.6551, which is larger than 1.6542 of C2. Well-defined layered structure of $LiNi_{0.5}Co_{0.2}Mn_{0.3}O_2$ material has the *c/3a* ratio of 1.6548 - 1.650.[2,12,33] The ratio of C1 is close to that known value. Splitting of the peaks of (006)/(102) and (108)/(110) is an indirect indication for the formation of a highly ordered layered structure like $LiCoO_2$.[34,35] The intensity ratio of $(I_{102}+I_{006})/I_{101}$for a perfect cation ordering is known to be 0.41 - 0.44.[36] Both C1 and C2 have 0.48. Another intensity ratio of I_{003}/I_{104} is indicative of undesirable cation mixing; the ratio lower than 1.2 indicates the migration of some Ni^{2+} ions to Li^+ sites and blocking of the channel of Li^+-ion transport.[37,38] While the ratio of I_{003}/I_{104} of C1 is 1.35, that of C2 is 1.07 due to cation mixing. All the factors indicate the C1 active material is crystallized in an ordered layered hexagonal structure.

Elemental mapping images for C1 (Figure 5b) demonstrate a sustained homogeneous distribution of constituent atoms in the bulk from the precursor P1. This emphasizes the importance of material characteristics of the coprecipitate precursor in tailoring and controlling the material properties of cathode active material. Size and shape of secondary particles of C1 remain unchanged from the precursor P1, as displayed in the SEM images in Figure 6a. On the contrary, for the C2, spherical secondary particles did not form and particle shape and size are irregular. As the P2 has already a disordered structure of layered hydroxide, it results in the poor crystallinity and irregular particle size and shape of primary particles.

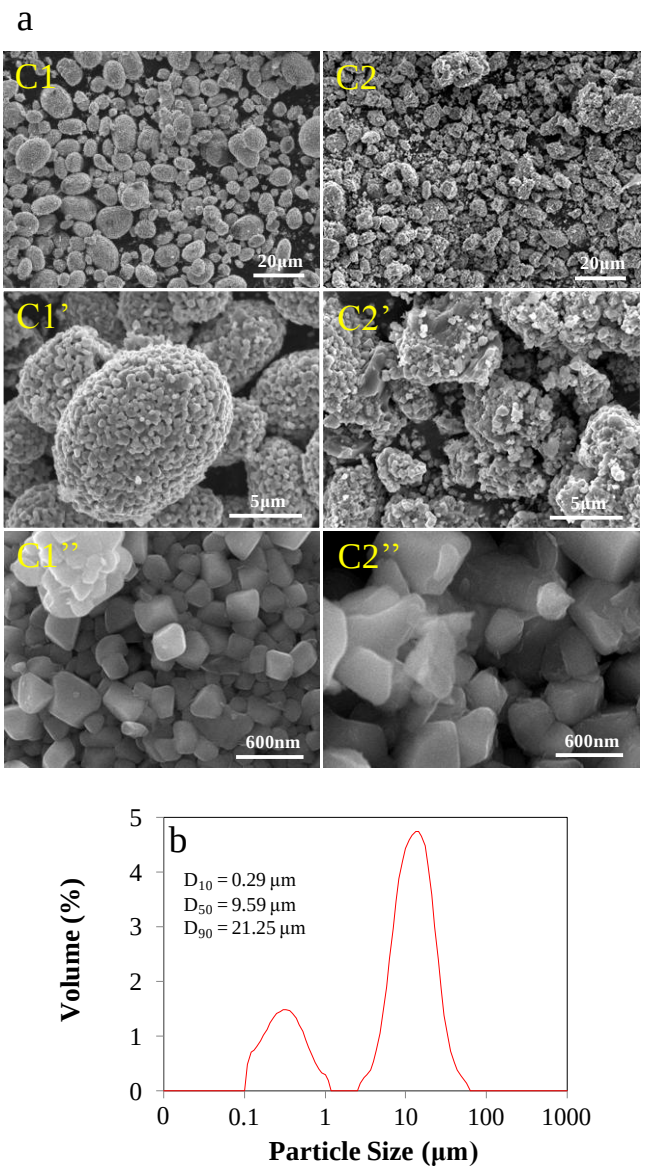

Figure 6. SEM images (a) of $LiNi_{0.5}Co_{0.2}Mn_{0.3}O_2$ cathode active materials of C1 and C2 at different magnification, and (b) particle size distribution of C1.

In the course of high temperature calcination of P2 with LiOH for the synthesis of C2, secondary particles of P2 seem to crack. Also during the calcination for the synthesis of cathode active material at 900 ^oC in the air, thermal energy causes the decomposition of residual citrate and evaporation of CO_2 gas.[39] Then, primary particles are scattered and their adherence weakens. The more citrate is used, the less ordered and stacked primary and secondary particles.

Figure 6b shows the particle size distribution of C1 active material. The D_{50} of C1 is 9.59 μm, corresponding to the size of secondary particles. D_{50} is known as the medium value of the

particle size distribution, which indicates the particle diameter at the fraction of 50 % in the cumulative distribution. Main particle size that occupies the fraction of 76 % is ~13 μm. However, as observed

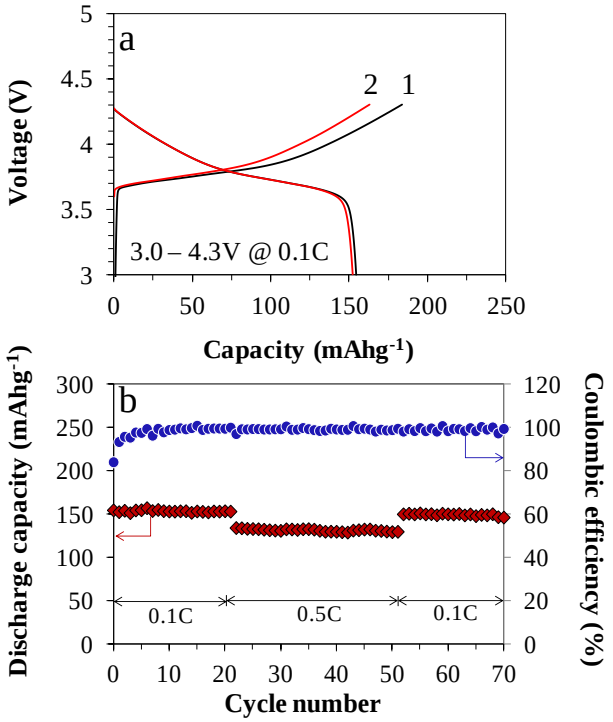

Figure 7. Voltage profile (a) and cycling ability (b) of Li//$LiNi_{0.5}Co_{0.2}Mn_{0.3}O_2$ cell in 1M $LiPF_6$/EC:EMC in the voltage range of 3.0 - 4.3 V.

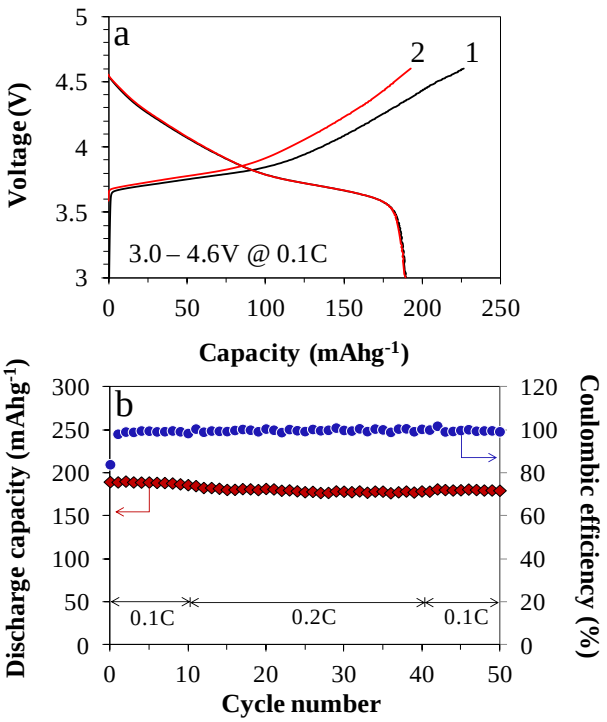

Figure 8. Voltage profile (a) and cycling ability (b) of Li//$LiNi_{0.5}Co_{0.2}Mn_{0.3}O_2$ cell in 1M $LiPF_6$/EC:EMC with 5wt% FEMC additive in the voltage range of 3.0 - 4.6 V.

in Figure 6a, there are smaller particles with the diameter of ~1 μm, which accounts for the fraction of 24 % of the total particles. The tap density of C1 active material was 2.31 gcm^{-3}. It is slightly lower than 2.6 gcm^{-3} of commercialized $LiCoO_2$,[40,41] Further improvements can be made to increase the tap density of cathode material by optimizing the stirring speed, reaction time, etc. for coprecipitation synthesis.

Electrochemical charge-discharge cycling ability of C1 of $LiNi_{0.5}Co_{0.2}Mn_{0.3}O_2$ cathodes, which was prepared from the coprecipitate precursor P1, was tested in 2016 lithium coin half-cells. In the voltage region of 3.0 and 4.3 V, the cell was tested in the electrolyte of 1M $LiPF_6$/EC:EMC at the rates of 0.1C (18 mAg^{-1}), 0.5C (90 mAg^{-1}) and 0.1C again. The initial charge and discharge capacities at 0.1C (Figure 7a-b) are 183 and 154 $mAhg^{-1}$, respectively, resulting in the initial coulombic efficiency of 84 %. At 0.5C (Figure 7b), the cathode still shows the discharge capacity of 134 $mAhg^{-1}$ and excellent reversibility. Excellent capacity retention of 95 % with the discharge capacity of 146 $mAhg^{-1}$ was obtained after 70 cycles. The rate of capacity fade at 0.1C is very low, 0.12 $mAhg^{-1}$ per cycle. This demonstrates similar cycling performance upon charging to 4.3 V to that of the cathodes that were synthesized using the precursor produced *via* ammonia-containing coprecipitation.[13,42-45]

High-voltage cycling ability of cathode in the voltage region of 3.0 – 4.6 V was conducted in the electrolyte with 5 wt % FEMC as a high-voltage additive at the rates of 0.1C, 0.2C and 0.1C again for possible high-energy density battery applications. As displayed in Figure 8a-b, initial charge and discharge capacities at 0.1C are 226 and 189 $mAhg^{-1}$, respectively, corresponding to initial coulombic efficiency of 84 %. At 0.2C (Figure 8b), the cathode maintains high discharge capacities of 185 - 179 $mAhg^{-1}$ from 11th to 40th cycle, exhibiting a great capacity retention of 94 % at the 50th cycle and a low rate of capacity fade of 0.25 $mAhg^{-1}$ per cycle at 0.1C. This high-voltage cycling performance is comparable to that of the cathodes that used the precursor produced *via* ammonia-containing coprecipitation.[30,42]

Conclusions

Homogeneous multicomponent metal hydroxides coprecipitate precursor of $Ni_{0.5}Co_{0.2}Mn_{0.3}(OH)_2$ with tailored particle size and shape was synthesized *via* ammonia-free and low-cost green coprecipitation process, using citric acid as a new chelating agent. Through the theoretical consideration of thermodynamic equilibrium of various chemical species in aqueous solution, the optimum pH 10.5 – 11.5 for the coprecipitation of $Ni_{0.5}Co_{0.2}Mn_{0.3}(OH)_2$ was determined. The use of a relatively low content of citric acid to metal is effective in producing crystalline metal hydroxides with spherical shape and size (5 - 15 μm) of secondary particles that consist of primary particles in the diameter of 300 - 500 nm. Cathode active material of $LiNi_{0.5}Co_{0.2}Mn_{0.3}O_2$, which was synthesized using the precursor of $Ni_{0.5}Co_{0.2}Mn_{0.3}(OH)_2$, exhibits a maintained particle size and spherical shape of the precursor. Moreover, lithium cells with the synthesized cathode active material of $LiNi_{0.5}Co_{0.2}Mn_{0.3}O_2$ showed an excellent charge-discharge cycling performance. This demonstrates that our environmentally friendly coprecipiation synthesis provides appropriate material characteristics of

$Ni_{0.5}Co_{0.2}Mn_{0.3}(OH)_2$ coprecipitate precursor, which leads to suitable material properties of cathode active material as well and its good battery performance.

Acknowledgements

This work was supported partly by the Small and Medium Business Technology Innovation Development Program (S2045224) and partly by the Ministry of Education (2012026203) of Korea.

Notes and references

1 Z. L. Liu, A. S. Yu and J. Y. Lee, *J. Power Sources*, 1999, **81**, 416–419.
2 T. Ohzuku and Y. Makimura, *Chem. Lett.*, 2001, **30**, 642–643.
3 N. Yabuuchi and T. Ohzuku, *J. Power Sources*, 2003, **119**, 171–174.
4 X. Luo, X. Wang, L. Liao, S. Gamboa and P. J. Sebastian, *J. Power Sources*, 2006, **158**, 654–658.
5 C. Deng, L. Liu, W. Zhou, K. Sun and D. Sun, *Electrochim. Acta*, 2008, **53**, 2441–2447.
6 Z. Lu, D. D. MacNeil and J. R. Dahn, *Electrochem. Solid-State Lett.*, 2001, **4**, A191–A194.
7 A. V. Bommel and J. R. Dahn, *Chem. Mater.*, 2009, **21**, 1500-1503.
8 M. H. Lee, Y. J. Kang, S. T. Myung and Y. K. Sun, *Electrochim. Acta*, 2004, **50**, 939–948.
9 J. Ying, C. Jiang and C. Wan, *J. Power Sources*, 2004, **129**, 264–269.
10 A. V. Bommel and J. R. Dahn, *J. Electrochem. Soc*., 2009, **156**, A362-A365.
11 N. V. Kosova, E. T. Devyatkina and V. V. Kaichev, *J. Power Sources*, 2007, **174**, 735–740.
12 M. Noh and J. Cho, *J. Electrochem. Soc*., 2013, **160**, A105-A111.
13 S. Yang, X. Wang, X. Yang, Z. Liu, Y. Bai, Y. Wang and H. Shu, *J. Solid State Electrochem.*, 2012, **16**, 2823–2836.
14 B.-R. Lee, H.-J. Noh, S.-T. Myung, K. Amine and Y.-K. Sun, *J. Electrochem. Soc.*, 2011, **158**, A180-A186.
15 J. Cho, *Chem. Mater.*, 2000, **12**, 3089-3094.
16 G. Ruiz, D. Jeison and R. Chamy, *Water Res.*, 2003, **37**, 1371–1377.
17 W. Jianlong and Y. Ning, *Process Biochem.*, 2004, **39**, 1223–1229.
18 I. Murray, J. W. Parsons and K. Robinson, *Water Res.*,1975, **9**, 25–30.
19 Y.-H. Ahn, *Process Biochem.*, 2006, **41**, 1709–1721.
20 J. N. Smith, A. D. Keil, R. J. Noll and R. G. Cooks, *Analyst*, 2011, **136**, 120–127.
21 R. Y. Ying and P. K. Ng, *J. Electrochem. Soc.*, 1988, **135**, 2964-2971.
22 Y. S. Han, S.-W. Song, S. H. Chang and J. H. Choy, *J.Mater. Chem.*, 1994, **4**, 1271–1274.
23 H. Gamsjäger, H. Wallner and W. Preis, *Monatsh. Chem.*, 2002, **133**, 225–229.
24 W. Stumm and J. J. Morgan in *Aquatic Chemistry: Chemical Equilibria and Rates in Natural Waters, John Wiley & Sons, Vol. 3* (Eds.: J. L. Schnoor, A. Zehnder), Wiley, New York, USA , 1996, pp325–334.
25 D. R. Turner, M. Whitfield and A. G. Dickson, *Geochim. Cosmochim. Acta*, 1981, **45**, 855–881.
26 N. V. Plyasunova, Y. Zhang and M. Muhammed, *Hydrometallurgy*, 1998, **48**, 43–63.
27 Y. Xiang, Z. Yin and X. Li, *J. Solid State Electrochem*., 2014, **18**, 2123-2129.
28 K. Yang, L.-Z. Fan, J. Guo and X. Qu, *Electrochim. Acta*, 2012, **63**, 363–368.
29 S. Yang, X. Wang, X. Yang, Y. Bai, Z. Liu, H. Shu and Q. Wei, *Electrochim. Acta*, 2012, **66**, 88– 93.
30 Y.-M. Lee, K.-M. Nam, E.-H. Hwang, Y.-G. Kwon, D.-H. Kang, S.-S. Kim and S.-W. Song, *J. Phys. Chem. C*, 2014, **118**, 10631–10639.
31 X. Xiao, J. Lu and Y. Li, *Nano Res.*, 2010, **3**, 733–737.
32 T. N. Ramesh, M. Rajamathi and P. V. Kamath, *Solid State Sci.*, 2003, **5**, 751–756.
33 J. K. Ngala, N. A. Chernova, M. Ma, M. Mamak and P. Y. Zavalij, *J. Mater. Chem.*, 2004, **14**, 214–220.
34 Y. Gao, M. V. Yakovleva and W. B. Ebner, *Electrochem. Solid State Lett.*, 1998, **1**, 117–119.
35 K. M. Shaju, G. V. S. Rao and B. V. R. Chowdari, *Electrochim. Acta*, 2002, **48**, 145–151.
36 J. N. Reimers, E. Rossen, C. D. Jones and J. R. Dahn, *Solid State Ionics*, 1993, **61**, 335–344.
37 Y. Fujita, K. Amine, J. Maruta and H. Yasuda, *J. Power Sources*, 1997, **68**, 126–130.
38 X.-Z. Fu, X. Wang, H.-F. Peng, F.-S. Ke, J.-H. Lei, L. Huang, J.-D. Lin and D.-W. Liao, *J. Solid State Electrochem.*, 2010, **14**, 1117–1124.
39 N. S. Gajbhiye and S. Prasad, *Thermochim. Acta*, 1996, **285**, 325–336.
40 J. Ying, C. Jiang and C. Wan, *J. Power Sources*, 2004, **129**, 264–269.
41 P. He, H. Wang, L. Qi and T. Osaka, *J. Power Sources*, 2006, **158**, 529–534.
42 J. Shu, R. Ma, L. Shao, M. Shui, K. Wu, M. Lao, D. Wang, N. Long and Y. Ren, *J. Power Sources*, 2014, **245**, 7−18.
43 S.-B. Kim, K. J. Lee, W. J. Choi, W.-S. Kim, I. C. Jang, H. H. Lim and Y. S. Lee, *J. Solid State Electrochem.*, 2010, **14**, 919–922.
44 K. Wu, F. Wang, L. Gao, M.-R. Li, L. Xiao, L. Zhao, S.Hu, X. Wang, Z. Xu and Q. Wu, *Electrochim. Acta*, 2012, **75**, 393–398.
45 H.-J. Noh, S. Youn, C. S. Yoon and Y.-K. Sun, *J. Power Sources*, 2013, **233**, 121-130.

Ammonia-Free Coprecipitation Synthesis of Ni-Co-Mn Hydroxides Precursor for High-Performance Battery Cathode Materials

Kyoung-Mo Nam, Hyun-Jin Kim, Dong-Hyun Kang, Yong-Seok Kim and Seung-Wan Song

A graphical and textual abstract for the Table of contents entry

Ammonia-free coprecipitation process using citric acid as a new chelating agent successfully produced micro-sized spherical $Ni_{0.5}Co_{0.2}Mn_{0.3}(OH)_2$ precursor and well-performed cathode active material of $LiNi_{0.5}Co_{0.2}Mn_{0.3}O_2$ for Li-ion batteries.